Novel approach for measurement of restitution coefficient by magnetic particle tracking

Tobias Oesau [a,*], Philipp Grohn [b], Swantje Pietsch-Braune [a], Sergiy Antonyuk [b], Stefan Heinrich [a]

[a] Institute of Solids Process Engineering and Particle Technology, Hamburg University of Technology, Denickestrasse 15, 21073 Hamburg, Germany
[b] Institute of Particle Process Engineering, Technische Universität Kaiserslautern, Gottlieb Daimler Strasse, 67663 Kaiserslautern, Germany

ARTICLE INFO

ABSTRACT

Inter particular contacts between particles are of great interest, as the intensity and quantity of contacts impact the behavior of a wide variety of industrial processes. The coefficient of restitution is commonly used to describe the collision of a particle either with other particles or with walls and components of plant equipment. The coefficient considers the amount of energy that is dissipated in the collision event. Usually the restitution coefficient is examined by the use of high speed cameras and image velocimetry. In this study a new method based on magnetic particle tracking (MPT) was developed to measure the restitution coefficient of magnetic particles. By performing simultaneous image velocimetry and MPT measurements, the novel approach is validated. The comparison shows a high coincidence of the results from both measurement methods, both for normal direction impacts as well as impacts on oblique surfaces. Furthermore, the rotation of particles was investigated (by rolling down a tilted plate), which has also shown the applicability of the MPT measurement method.

© 2021 The Society of Powder Technology Japan. Published by Elsevier BV and The Society of Powder Technology Japan. This is an open access article under the CC BY-NC-ND license (http://creativecommons.org/licenses/by-nc-nd/4.0/).

1. Introduction

A wide variety of products from chemical, pharmaceutical or food industry are processed by the handling of particulate raw products. The commonly used production processes, e.g. mixers or fluidized beds, are mainly characterized by the high number of interparticular contacts between the particles. As the properties of the products rely not only on the process and material parameters but on the amount and intensity of the interparticular contacts as well, the knowledge of the collision dynamics is highly important for the understanding and design of the process. As it was shown by Seville et al. [39] and van Buijtenen et al. [44], a change of the collision dynamics on the micro-scale influences the behavior on the macro-scale as well.

Due to ever increasing computing power, the modeling of dense solid–gas flows by coupled CFD-DEM simulations gains in importance [17]. DEM is a numerical approach for the calculation of movement and interactions of individual elements (particles or drops) by Newtonian and Eulerian movement equations. The dynamics of the single particle as well as of the particle collective can be analyzed and traced temporally. With this method it is also possible to take the rotation of the particles, the influence of adhesive forces due to liquid or solid bridges and the irregular shape of the particles into account, which can not be done by other modeling approaches. In DEM the complex and short-time interactions between interacting particles and between particles and components of the plant are described by different approaches. For inelastic material behavior the energy adsorption during the collision is considered in a DEM contact model by the coefficient of restitution (CoR). The coefficient of restitution was introduced by Newton [32] and describes the ratio of the rebound and impact energies of the collision partners [1,5,16,23,25,26,33,40,41,47].

The restitution coefficient is commonly measured by two main types of experiments: The first type is the pendulum experiment, where a particle is placed at the end a pendulum and impacts either on a wall [14,21] or onto a second particle [20,40]. By comparing the angle of deflection before and after the collision, the restitution coefficient can be obtained. This method was already established back in the eighties by Bridges et al. [6] and Hatzes et al. [19]. Kantak et al. [22] determined the restitution coefficient with this method for normal directed impacts, while Seifried et al. [37,38] examined the restitution coefficient during repeated impacts. As shown by Hlosta et al. [20] the pendulum based method is able to produce good results for irregular shaped particles, however the particle diameters were quite large ($d_p > 5$ mm). Furthermore the stiffness of the pendulum wires

---

* Corresponding author.
  E-mail address: tobias.oesau@tuhh.de (T. Oesau).

Nomenclature

Abbreviations

AMR	Anisotropic magneto resistive
CFD	Computational fluid dynamics
CoR	Coefficient of restitution
DEM	Discrete element method
MPT	Magnetic particle tracking
NdFeB	Neodymium iron boron
PVB	Polyvinyl butyral
ZrO_2	Zirconium dioxide

Other symbols

$\boldsymbol{B}$	Magnetic flux density (T)
$\boldsymbol{D}$	Electric displacement field ($As\,m^{-2}$)
$\boldsymbol{E}$	Electric field ($V\,m^{-1}$)
$\boldsymbol{E}_n$	Unity vector at time point n
$\boldsymbol{H}$	Magnetic field ($A\,m^{-1}$)
$\boldsymbol{j}$	Current density ($A\,m^{-2}$)
$\boldsymbol{R}$	Position vector (m)
$\boldsymbol{r}_i$	relative position vector (m)
$\boldsymbol{u}_n$	Velocity vector at time point n ($m\,s^{-1}$)
μ	Magnetic moment ($A\,m^{-2}$)
ω	Rotational velocity ($rad\,s^{-1}$)

ϕ_p	Angle between two unity vectors (rad)
ρ	Electric charge density ($C\,m^{-3}$)
$\rho_{core,i}$	Density of the core material ($kg\,m^{-3}$)
d_{coated}	Diameter of the coated material (m)
d_{core}	Diameter of the core material (m)
e	Total coefficient of restitution (-)
E_{diss}	Dissipated energy (J)
e_n	Normal coefficient of restitution (-)
E_i	Alignment values (i = x,y or z)
$E_{kin,0}$	Kinetic energy before impact (J)
$E_{kin,R}$	Kinetic energy during rebound (J)
h_0	Height before impact (m)
h_R	Rebound height (m)
J	Moment of inertia ($kg\,m^2$)
Q	Quality function (-)
t_n	Time point (s)
v_0	Impact velocity ($m\,s^{-1}$)
v_n	Normal velocity ($m\,s^{-1}$)
v_R	Rebound velocity ($m\,s^{-1}$)

Physics constants

g	Gravitational acceleration ($m\,s^{-2}$)

has to be known and taken into account for the measurement. In addition it is only possible to measure the coefficient of restitution without initial rotation of the contact partners.

The second common type for the determination of the restitution coefficient is the free-fall experiment. In this, a particle is held on a defined height over a plate or a second particle by a vacuum nozzle. By releasing the vacuum, the particle falls downwards, only accelerated by gravity. A simple approach to determine the coefficient of restitution in this setup is the comparison of the rebound height to the height, from which the particle was released, if the drag and buoyancy forces can be neglected. For both types of experiments was shown that it is advantageous to monitor the experiment by high-speed cameras, as the determination of the respective values is more precisely by camera and the velocities of the particles can be obtained rather than the heights before and after the impact. Furthermore, a determination of the rotation of particles is possible by the use of cameras. However, the analysis of the measurement data can be complex if the particles are not spherical or when the impact and rebound path are in different planes, as this requires a 3D monitoring of the experiment by the use of at least one additional camera. The usually used high-speed cameras are very light sensitive. This requires a strong and homogeneous illumination of the particle and the experimental setup. For some systems it can be difficult to achieve these conditions, for example transparent particles or nontransparent fluids. The size of the particles that can be captured is limited by the optical resolution of the used cameras. Furthermore, the small depth of field of the high-speed cameras provides further challenges, as the particles need to collide exactly in the focus plane of the camera, whereas oblique impacts can lead to blurry images of the particle. With all these limitations, high speed image velocimetry is not suited for in situ measurements of particle collisions in dense solid–gas flows.

Extensive studies regarding the restitution coefficient have been performed by our group, for both normal [3,28,29] and tangential impacts [5,15,46]. An overview of the influence of liquid on the collision behavior for non-porous glass beads is given by Buck [7] for a wide range of experimental parameters [8–11], while

Antonyuk et al. [4] and Grohn et al. [18] examined the influence of the water content of porous particles on the coefficient of restitution.

In this work a novel approach to measure the restitution coefficient is presented. For the determination of the restitution coefficient free-fall experiments have been performed, which have been monitored by the magnetic particle tracking (MPT) technology. This technology is generally used for the analysis of 3D flow behavior of bulk materials and shear behavior in fluidized beds [12,13,30,31]. With MPT the magnetic field of a permanent dipole magnet tracer particle is detected. The method can be used for the measurement of the 3D trajectory and orientation of the tracer particle, which allows the measurement of the CoR for particles of complex shape and with initial rotation as well. Furthermore, the MPT technology can be used as an in situ measurement method, which allows the measurement in plants with complex wall geometries. The behavior of the detected tracer particle can be assumed to be representative for the whole particle collective, if the tracer and the bulk particles possess similar properties and collision behavior. To achieve similar surface properties, a coating of both the tracer particle and the bulk particles with a polymer was performed in our previous work by Neuwirth et al. [31]. The same approach was used in our work to homogenize the magnetic tracer and the bulk particles (ceramics). The results of this homogenization will be presented as well.

By comparing results obtained by conventional high-speed image velocimetry with the results from the novel approach based on the application of MPT for the determination of the restitution coefficient, the ability of the method for further measurements is evaluated.

2. Theory

In this chapter an overview of the theoretic background regarding the coefficient of restitution as well as the magnetic particle tracking technology is given.

2.1. Coefficient of restitution

The coefficient of restitution describes the energy dissipation E_{diss} during particle collisions and is defined as the ratio of the kinetic energy after ($E_{\text{kin,R}}$) and before the collision ($E_{\text{kin,0}}$):

$$e = \sqrt{\frac{E_{\text{kin,R}}}{E_{\text{kin,0}}}} = \sqrt{\frac{E_{\text{kin,0}} - E_{\text{diss}}}{E_{\text{kin,0}}}} = \sqrt{1 - \frac{E_{\text{diss}}}{E_{\text{kin,0}}}} \tag{1}$$

This equation can be simplified to the ratio of the impact and rebound velocities, if the change of the mass of the particle (m_{p}) during the collision is negligible:

$$e = \sqrt{\frac{E_{\text{kin,R}}}{E_{\text{kin,0}}}} = \sqrt{\frac{0.5\, m_{\text{p}}\, v_{\text{R}}^2}{0.5\, m_{\text{p}}\, v_0^2}} = \left| \frac{v_{\text{R}}}{v_0} \right| \tag{2}$$

Furthermore, the coefficient of restitution can be determined for normal, tangential and rotational rebound behavior. The CoR for a normal rebound of a particle from a wall is defined as the ratio of the normal velocities of the particle after and before the collision:

$$e_{\text{n}} = \left| \frac{v_{\text{n,R}}}{v_{\text{n,0}}} \right| \tag{3}$$

Another possibility to determine the coefficient is the use of the heights before and after the impact (h_0 and h_{R} respectively). With the assumption that the drag and buoyancy of the particle is negligible, the following equation can be used:

$$e_{\text{n}} = \left| \frac{v_{\text{n,R}}}{v_0} \right| = \frac{\sqrt{2\, g\, h_R}}{\sqrt{2\, g\, h_0}} = \sqrt{\frac{h_R}{h_0}} \tag{4}$$

2.2. Fundamentals of Magnetic Particle Tracking

The principle of the magnetic particle tracking method is based on the continuous detection of a dipole magnet. The quasi-static magnetic field around the magnet is analyzed by sensors. The measurement principle of the sensors is the anisotropic magneto-resistive effect. The electric resistance inside the sensors changes when the orientation and/or the strength of the magnetic field changes. Therefore, it is possible to measure not only the translational movement of the magnet, but also the rotation.

A schematic illustration of the system is given in Fig. 1. The system can have six degrees of freedom [35]: three translational degrees in each spatial direction (x, y and z) as well as two degrees for rotation around the x- and y-axis. As the magnetic field does not change for a rotation around the z-axis, this rotation is no degree of freedom and can not be measured.

Albeit being the sixth degree of freedom, the magnetic moment μ of the dipole magnet is often known, therefore the detection of

Fig. 1. Schematics of the spatial location and magnetic field distribution of the dipole magnet in relation to the sensor and to the point of origin as well as the two rotation axes of the magnet [31].

the dipole magnet is reduced to a five degrees of freedom problem. The foundation for the solution of the problem are Maxwell's equations [27], which describe the properties of an electromagnetic field:

$$\text{rot}\, \boldsymbol{H} = \frac{\partial \boldsymbol{D}}{\partial t} + \boldsymbol{j},$$

$$\text{rot}\, \boldsymbol{E} = \frac{\partial \boldsymbol{B}}{\partial t},$$

$$\text{div}\, \boldsymbol{D} = \rho, \tag{5}$$

$$\text{div}\, \boldsymbol{B} = 0,$$

with the magnetic field strength $\boldsymbol{H}$, the electric field strength $\boldsymbol{E}$, the electric displacement field $\boldsymbol{D}$, the magnetic flux density $\boldsymbol{B}$, the current density $\boldsymbol{j}$ and the electric charge density ρ. For a dipole magnet the Maxwell equations can be summarized into the following equation [2,35]:

$$\boldsymbol{H}(\boldsymbol{r}_i - \boldsymbol{R}, \mu) = \frac{1}{4} \left(-\frac{\mu}{r^3} + \frac{3[\mu(\boldsymbol{r}_i - \boldsymbol{R})] \cdot [(\boldsymbol{r}_i - \boldsymbol{R})]}{r^5} \right) \tag{6}$$

With this formula it is possible to describe the magnetic field $\boldsymbol{H}$ of a dipole magnet by the relative position vector $\boldsymbol{r}_i - \boldsymbol{R}$ of the magnet to the sensor and the magnitude of this vector r as well as by the position vector $\boldsymbol{R}$ in relation to the point of origin of the system. As already mentioned, the magnetic moment of the magnet is often known, therefore five degrees of freedom remain, which means that the number of sensors has to exceed the number of five. The solution of Eq. 6 represents a problem that has to be solved inversely by a non-linear optimization algorithm [34]. The quality of the solution of the optimization algorithm can be described by the quality function Q, which is given by the following equation:

$$Q = \sum_{i=1}^{N} \left(\boldsymbol{H}_{(\boldsymbol{r}_i - \boldsymbol{R}, \mu), i}^{\text{sensor}} - \boldsymbol{H}_{(\boldsymbol{r}_i - \boldsymbol{R}, \mu), i}^{\text{simulation}} \right)^2 \tag{7}$$

The qualitiy function is the sum of the squared difference between the measured magnetic field $\boldsymbol{H}_{(\boldsymbol{r}_i - \boldsymbol{R}, \mu), i}^{\text{sensor}}$ and a simulated magnetic field $\boldsymbol{H}_{(\boldsymbol{r}_i - \boldsymbol{R}, \mu), i}^{\text{simulation}}$ for each of the N sensors of the system. The optimization algorithm is repeated until the quality function reaches a certain, pre-set minimum value.

3. Methodology

For the MPT analysis an existing MPT sensor array arrangement, provided and constructed by the companies *Matesy GmbH* and *INNOVENT e. V.*, around a lab-scale rotor granulator is used. A rotary granulator is a special fluidized bed, which consists of a rotating disk instead of a distributor plate allowing the additional introduction of shear forces into the particle movement. The air stream, that is powered by a suction fan, can pass through the adjustable gap between the plate and the wall [24,43,45]. The MPT sensors are placed around the cylindrical process chamber with a diameter of 280 mm and a height of 300 mm. The process chamber walls and the rotor plate are made out of PMMA (thickness 10 mm). Furthermore all metallic parts of the plants are made by either aluminum or brass. Therefore, no ferromagnetic materials are present, which reduces the risk of unwanted interferences during MPT measurements, such as induced magnet fields or magnetic resistances. As the array is tailor-made for the rotor granulator experimental setup, it is advantageous to perform the experiments inside the plant as well. The complete setup can be seen in Fig. 2. The sensor
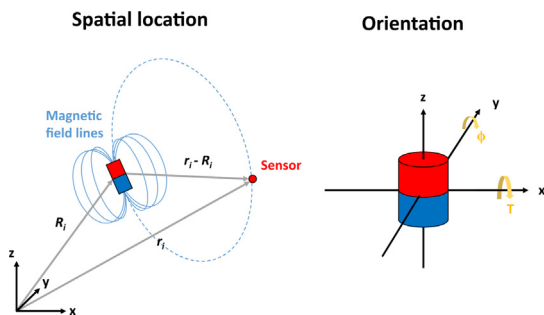
array consists of 24 sensor plates on four levels, with 72 anistropic magneto resistive (AMR) sensors in total. The data values from the sensors are logged and evaluated by a data logger and a computer with a measurement frequency of 1000 Hz. The spatial resolution of the measurement is down to 0.1 mm.

3.1. Materials and particle production

The subsequently described particles are suited for MPT measurements of the rotary granulator process, which will be performed beyond the scope of this work. As neodym magnets (NdFeB) show the highest magnetic field strengths, spherical particles of this material were used as tracer material. The magnetic moment of the particles strongly depends on the volume and therefore on the diameter of the sphere. The magnetic field of the tracer particle has to be strong enough to be detectable by the sensors. In experiments performed by Neuwirth et al. [31] a tracer diameter of 4.2 mm was used. Our recent early experiments have shown that the minimum diameter that can be used is 2 mm for the tracer core particles without a significant drop in the quality of the detection. The bulk material has to show similar properties (diameter and density) as the tracer particles to minimize segregation effects. Furthermore the contact behavior has to be similar, to guarantee similar particle dynamics. As the NdFeB magnets have very high density of 7200 kg m^{-3}, the bulk materials need a similar high density. Zirconium dioxide (ZrO$_2$) with a density of 6000 kg m^{-3} has proven to be a good candidate. To minimize the density differences and produce similar surface properties for all particles, both the tracer and the bulk particles were coated with polyvinyl butyral (PVB) with a density of 1100 kg m^{-3} (*Polyvinylbutyral 30* from *Kremer Pigmente*). For example, the magnetic NdFeB cores and the ZrO$_2$ particles with a diameter of 3 mm were coated with PVB up to a diameter of 4.2 mm. This diameter was chosen, because the difference in the moment of inertia between coated tracer and bulk particles drops below 10 percent at this value. An overview of the particle types and sizes, examined in this work,

is given in Table 1. The coating of the particles was performed in a spouted bed process, which has been used successfully earlier [36,42], where a 4 wt.% solution of ethanol and PVB was sprayed onto the particles by a two-fluid nozzle in top-spray configuration.

3.2. Experimental setup and procedure

For the experimental determination of the coefficient of restitution, a free-fall measurement setup was built into the open process chamber of the rotor granulator. A high-speed camera was installed facing the experiment, which allowed a simultaneous measurement of the restitution coefficient by magnetic particle tracking and by image velocimetry ($f = 4000$ fps). The setup for the free-fall experiments consists of an aluminum frame, on which a vacuum tweezer can be placed in different heights. By turning the vacuum pump of the tweezer on the particle is held in this position. When the pump is turned off, the particle falls down onto the target plate made out of glass, which is located on top of a tilting table. The glass plate is 80 x 80 x 10 mm (W x L x H) in size, with an almost ideal elastic contact behavior. The setup is shown in Fig. 3. With this setup it was possible to run the following three experiment types, which are also illustrated in Fig. 4: Normal impact, oblique impact and rotation experiments. With the normal and oblique impact experiments the coefficient of restitution was determined, by the rotation experiments the rotational velocity ω was obtained. For the latter experiments the vacuum nozzle was placed directly on top of the tilting table, so that the particle hits the inclined target and rolls down after the release.

3.2.1. Normal and oblique impact experiments

The materials stated in Table 1 have been examined for three different drop heights: 5, 10 and 15 cm. As the bulk material is not magnetic, a magnetic particle tracking measurement was not possible, therefore only the high-speed camera was used. The measurements for the bulk particles have been performed for the comparison of bulk and tracer particles, which will be used for later measurements beyond this work. Furthermore the particles were examined for an oblique impact. Therefore, the tilting table was fixed at three different angles (15, 30 and 45°). For each angle the drop height was also changed accordingly to the normal impact experiments. Each measurement was repeated at least 10 times.

3.2.2. Rotation experiments

The tilting table was fixed at the same angles as before, with the respective particle being held on the top by the vacuum tweezer. When releasing the vacuum, the particle starts to roll down the glass plate, which is recorded by MPT and the high-speed cameras simultaneously. The particles were marked with several black dots, which allowed a tracking of the movement of the surface, which relates to the rotational velocity. Each measurement was repeated at least 10 times.

3.3. Data analysis

The high-speed camera images obtained during the measurement were converted into binary images. The particle, which appears white in the binary images, was tracked by using an algorithm solved with the MATLAB Image Processing Toolbox. The algorithm was already used and established by Buck [7]. By using the frame rate and the scale of a pixel of the image, the velocity of the particles was determined between every two frames during collision and rebound. The image in the contact point of particles with the target was detected and the velocities were averaged over a range of twenty pictures before and after the impact, respectively.
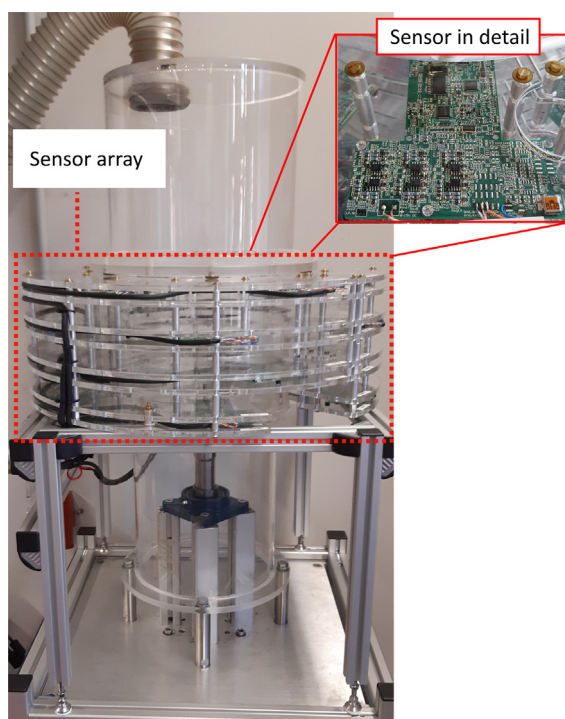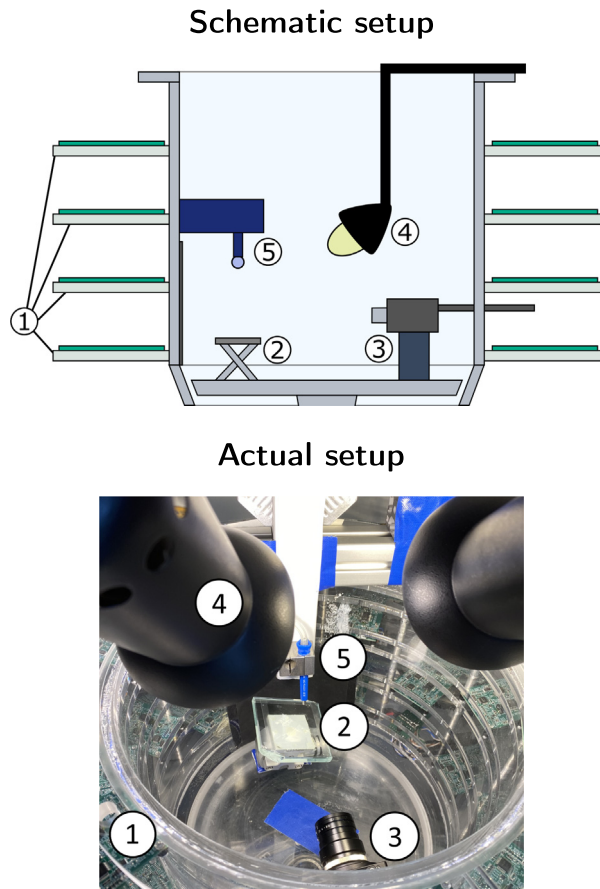

Fig. 2. Photo of the MPT sensor array around the process chamber of a lab-scale plant and detailed photo of one of the 24 sensor plates.
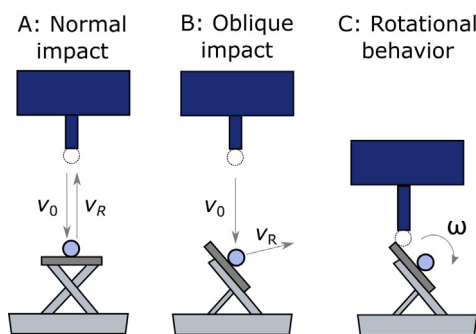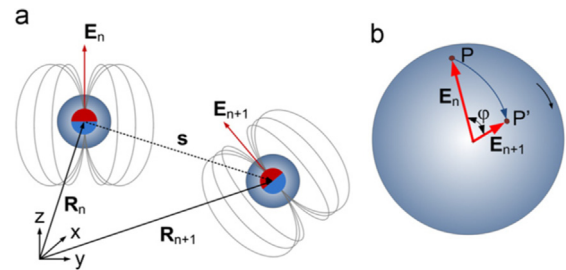
Table 1

Overview of the examined particles: respective diameters of the core particles and the diameters of the coated particles. All particles have been coated with PVB.

Type	Core material	$d_{\mathrm{core},i}$ in mm	$d_{\mathrm{coated},i}$ in mm	Density $\rho_{\mathrm{core},i}$ in $\mathrm{kg\,m^{-3}}$
Bulk	ZrO$_2$	2	2.8	6000
		3	4.2	
Tracer	NdFeB	2	2.8	7200
		3	4.2	

Schematic setup

Actual setup

Fig. 3. Top: Schematic drawing of the experimental setup Bottom: Photograph of the experimental setup. 1: MPT sensor array, 2: Tilting table with target glass plate, 3: High-speed camera, 4: Lights, 5: Particle and vacuum tweezer.

Experimental cases

Fig. 4. Schematic overview of the performed different test cases.

Fig. 5. Illustration of the dipole magnet for the determination of the: (a) translational velocity by position vectors $\mathbf{R}_i$ and (b) rotational velocity by unity vectors $\mathbf{E}_i$ [31].

3.3.1. Derivation of physical properties from the raw MPT measurement data

The measurement of the tracer is saved into a raw file, which contains the detected x-, y- and z-coordinates (in form of position vectors $\boldsymbol{R}_n$) of each time point t_n as well as the alignment values E_x, E_y and E_z of an unity vector $\boldsymbol{E_n}$, which are illustrated in Fig. 5. For the determination of the averaged translatoric velocity vector $\boldsymbol{u}_n$ a moving average method of eleven time points is used:

$$
\begin{aligned}
\boldsymbol{u}_n \;=\;& 0.10\,\frac{\mathbf{R}_{n+5}-\mathbf{R}_n}{t_{n+5}-t_n} + 0.15\,\frac{\mathbf{R}_{n+4}-\mathbf{R}_{n-1}}{t_{n+4}-t_{n-1}} \\
&+ 0.25\,\frac{\mathbf{R}_{n+3}-\mathbf{R}_{n-2}}{t_{n+3}-t_{n-3}} + 0.25\,\frac{\mathbf{R}_{n+2}-\mathbf{R}_{n-3}}{t_{n+2}-t_{n-3}} \\
&+ 0.15\,\frac{\mathbf{R}_{n+1}-\mathbf{R}_{n-4}}{t_{n+1}-t_{n-4}} + 0.10\,\frac{\mathbf{R}_n-\mathbf{R}_{n-5}}{t_n-t_{n-5}}
\end{aligned}
\tag{8}
$$

For the rotational velocity ω it is necessary to calculate the angle ϕ_p between the two magnetic axis unit vectors ($\boldsymbol{E}_n$ and $\boldsymbol{E}_{n+1}$):

$$
\phi_p = \cos^{-1}\left(\frac{\boldsymbol{E}_n \cdot \boldsymbol{E}_{n+1}}{|\boldsymbol{E}_n| \cdot |\boldsymbol{E}_{n+1}|}\right) \text{ in rad}
\tag{9}
$$

With the angle it is possible to calculate the velocity:

$$
\omega = \frac{\phi_p}{t_{n+1} - t_n} \text{ in rad s}^{-1}
\tag{10}
$$

The MPT measurement raw data were converted by an algorithm in MATLAB, which calculated the best solution for the location problem by averaging over eight measurement points, to reduce noise in the data. This reduces the actual measurement frequency from 1000 Hz down to an apparent frequency of 125 Hz. The converted data were analyzed subsequently with MATLAB as well. Due to lower frequency compared to the high-speed camera, the velocity was not averaged before and after the impact point. If the exact contact point was not obvious from the MPT data and the data deemed to be very noisy, the approach from Eq. 4 was used, and the heights before and after the impact were used, as the height could be analyzed easier than the velocities, if no contact point was obvious.

4. Results

First, the two different particle types, tracer and bulk material, are compared regarding their physical properties and their kinetic behavior, which is recorded solely by the high-speed cameras. This is important for later investigations in the rotary granulator. In a second step the two measurement techniques, MPT and high-speed image velocimetry are compared.

4.1. Comparison of tracer and bulk particle properties and collision dynamics

The first step of the comparison of the two particle types is the determination of physical properties of both particle types. Therefore, the density (via helium pycnometry, *AccuPyc 1330* from *Micromeritics*), the Young's modulus (by nanoindentation, *Hysitron TI Premier* from *Bruker Corporation*) and the calculated moment of inertia were determined. The moment of inertia for any given body independent of it's shape is generally defined by the following equation:

$$J = \frac{1}{3}(J_x + J_y + J_z)$$

By taking the rotational symmetry of a sphere into account, the equation is simplified to the following form [30]:

$$J_i = \frac{2}{3}\rho_{\text{core},i} \int_0^\pi \int_0^{2\pi} \int_0^{r_{\text{core},i}} r^4 \sin\theta \, dr \, d\phi \, d\theta$$
$$+ \frac{2}{3}\rho_{\text{PVB}} \int_0^\pi \int_0^{2\pi} \int_{r_{\text{core},i}}^{r_{\text{coated},i}} r^4 \sin\theta \, dr \, d\phi \, d\theta$$

The analytic solution of the aforementioned equation is given by:

$$J_i = \frac{8\pi}{15}\left[\rho_{\text{core},i} r_{\text{core},i}^5 + \rho_{\text{PVB}}\left(r_{\text{coated},i}^5 - r_{\text{core},i}^5\right)\right] \qquad (11)$$

The values for the radii $r_{\text{core},i}$ and $r_{\text{coated},i}$ as well as the densities $\rho_{\text{core},i}$ can be found in Table 1. The obtained values for the mentioned properties are shown in Table 2. The results are very similar for each particle size. As already described, the moment of inertia has only been theoretically calculated and differs by ten percent between the particle types, as the coating of the particles was stopped, when the desired diameters had been reached. As all values are very similar with a difference less than 15 percent, it can be assumed, that the physical properties of the particle types have been homogenized due to the coating. However, the restitution behavior has to be examined as well, to ensure that the particles behave similar during contacts as well.

The results for the coefficient of restitution during a normal impact are shown in Fig. 6. As it can be seen, the restitution coefficient is constant over the examined range of impact velocities. This was also shown by Antonyuk et al. [5] and Buck [7]. With the coefficient of restitution being higher than 0.8 and close to 0.9, the impact in these velocity ranges can be characterized as dominantly elastic. Comparing the results from the coated particles with the uncoated core particles, no significant decrease in
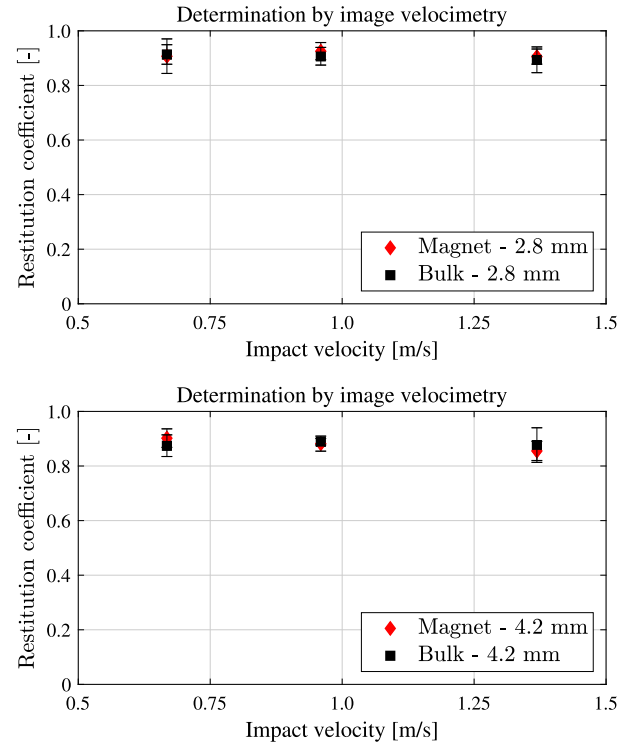
Table 2
Overview of physical properties for both particle types and different particle sizes.

Type	Density in kg m^{-3}	Young's modulus in GPa	Moment of inertia in g mm^2
Bulk 2.8	3485.4	2.04	0.018
Tracer 2.8	4035.8	1.96	0.020
Bulk 4.2	3581.8	1.68	0.131
Tracer 4.2	3927.2	1.78	0.157

Fig. 6. Comparison of the restitution coefficient for a normal impact onto a glass plate for the different particle types and particle sizes for different impact velocities.

the coefficient is measured. This confirms, that the coating of the particles did not change the behavior of the particles. As the velocities in the rotary granulator are known to be in the examined range, a dominant elastic behavior can be implied for the particles. Lastly, the results show that both particle types have very similar coefficients of restitution for the examined velocities, regardless of the particle diameter. All this proves that the different particle types behave very similar during impact, which concludes that their behavior in the rotary granulator processes are expected to be sufficiently similar.

4.2. Comparison of MPT and high-speed image measurements

To give a broader understanding of the measurement methods an exemplary analysis is performed at the start for both the high-speed image velocimetry and the MPT measurement. Exemplary images from the high-speed cameras are given in Fig. 7. By using the MATLAB algorithm, the course of the velocity in normal direction can be determined, which is illustrated in Fig. 8. As mentioned in Section 3.3, the contact point is detected (here: just before 15 ms) and the impact and rebound velocities are averaged over the 20 pictures captured before and after the contact.

In contrast, it was possible to measure the whole drop path for the tracer particles with MPT, which is shown in Fig. 9. Therefore the observed time period is much longer (500 ms for one impact compared to around 25 ms for the high-speed camera). However, the measurement frequency for the MPT measurements is much lower than for the cameras. This results in a significantly lower density of data points near the impact point. This means that higher deviations are possible, which lead to the use of the heights before and after the impact in Eq. 4.

Subsequently, the results for three different experiment types are presented.

Normal impact
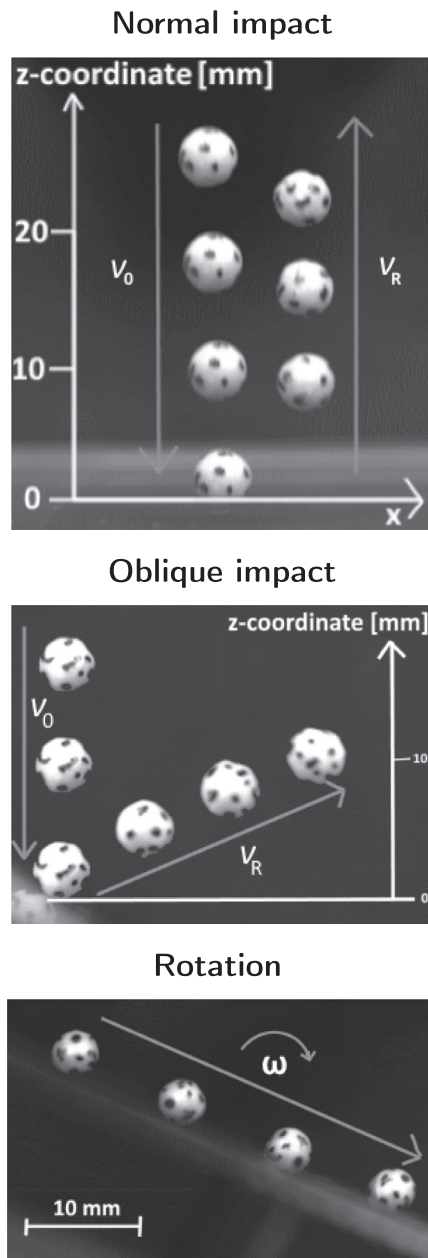

Oblique impact

Rotation

Fig. 7. Series of high-speed images merged into one picture for all three types of experiments. Top: 4.2 mm magnetic tracer particle onto a glass plate from 15 cm drop height. Middle: Oblique impact for the 4.2 mm magnetic tracer particle for a drop height of 15 cm and a tilting angle of 45°. Bottom: Rotation experiment for the 4.2 mm magnetic tracer particle with a tilting angle of 30°. For all pictures: between each particle a time of 5 ms has passed.

Fig. 8. Time dependent course of the velocity of the tracer particle obtained by high-speed cameras for a 4.2 mm tracer particle impact from a height of 15 cm onto a glass plate.

Fig. 9. Time dependent course of the z-coordinate of the tracer particle obtained by MPT for a 4.2 mm tracer particle from a height of 15 cm onto a glass plate.

the method of evaluation. As described in section 3.4, the velocity of the particle is obtained by significantly less data points compared to the image velocimetry. As the magnetic strength of the particle decreases sharply with decreasing diameter, the detection quality for the 2.8 mm particle was expected to be lower than for the 4.2 mm particle. This is reflected by the results, as the values by MPT for the smaller particles differ more from the values obtained by image velocimetry than the values for the bigger particles. As the results for the image velocimetry do not depend on the magnetic strength of the tracer, the difference can be explained by the lower detection quality. This is furthermore supported by the values obtained for the quality function, mentioned in Eq. 7. For the smaller particles, the quality function reached values around 0.1, while the values for the 4.2 mm particles were significantly lower (around 0.06), with the quality function showing a worse detection quality with higher values.

4.2.1. Normal impact

The results for the normal impact of the particles onto a glass plate are shown in Fig. 10. The values for the coefficient of restitution obtained by both measurement methods are very similar, as the highest difference between the measurements amounts to 8.5 % for the lowest impact velocity of 0.65 m s^{-1} (which corresponds to a drop height of 5 cm) for the 2.8 mm particles. For the bigger particles, the values show an even better agreement. The already established trend, that the velocity has no impact on the coefficient of restitution in the investigated range of impact velocities can also be seen in the MPT measurements, taking into account that the standard deviation of the results is higher than by high-speed camera measurements. This can be explained by
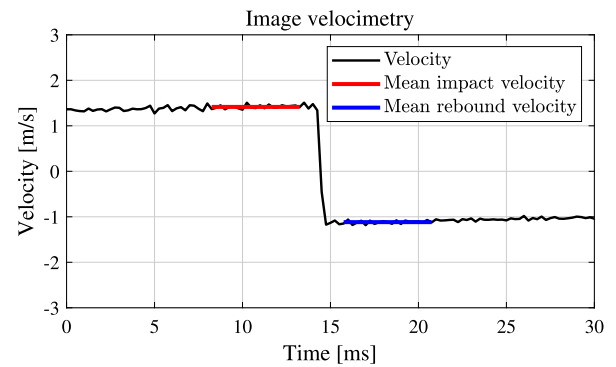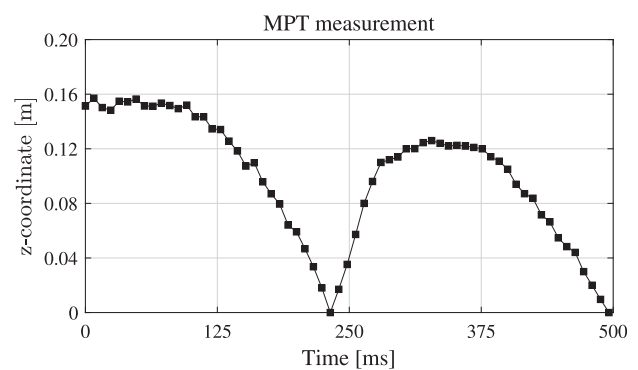
4.2.2. Oblique impact

The same experiments as in the previous section were performed, but for different tilting angles of the tilting table. The restitution coefficient shown in Fig. 11 is the total restitution coefficient, as the coefficient for an oblique impact can be divided into a normal and a translational component. Therefore, the total spatial velocity was determined and compared before and after impact. The results for the two particle sizes are presented in Fig. 11. Here, only the results for an impact speed of 1 m/s are shown, as further evaluations for 0.6 and 1.3 m/s did not conclude an impact of the velocity on the results. The values obtained by MPT show no significant influence of the impact angle on the total restitution coefficient as well, especially for the 4.2 mm particles, which coincides with earlier studies performed by Buck [7].
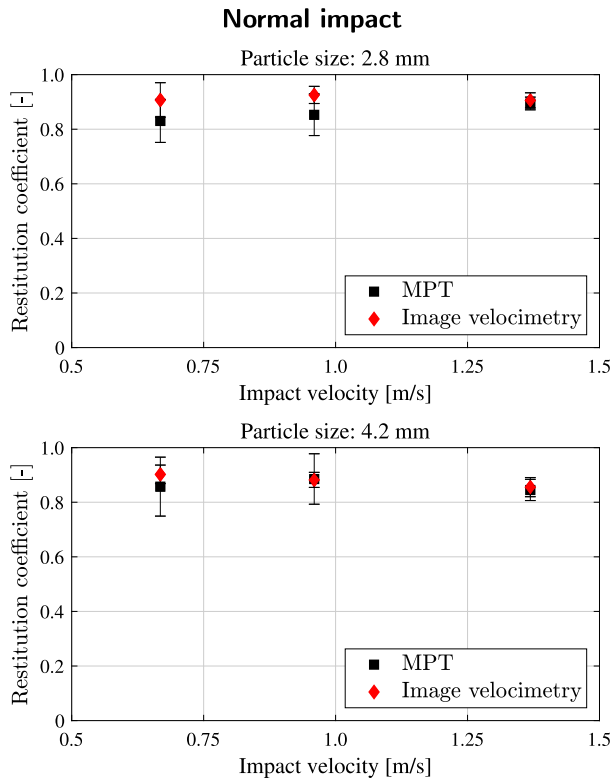
Normal impact

Fig. 10. Comparison of results for the coefficient of restitution of the tracer particle for a normal impact onto a glass plate, obtained by high-speed image velocimetry and MPT.
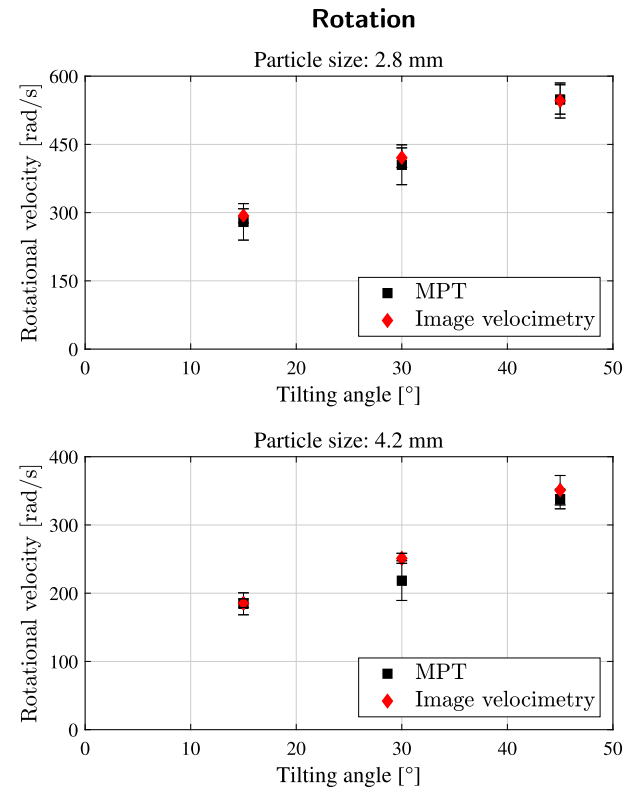
Oblique impact

Fig. 11. Comparison of results for the coefficient of restitution of the tracer particle for different impact angles onto a glass plate, obtained by high-speed image velocimetry and MPT for an impact velocity of 1 m/s.

Rotation

Fig. 12. Comparison of results for the rotational behavior of the tracer particle for different angles of the tilting table.

4.2.3. Rotational behavior

As the rotational velocity increases over time, the illustrated results in Fig. 12 represent an averaged velocity over the examined distance of 5 cm (compare with Fig. 7). For both particle sizes the velocity increases with higher tilting angle of the glass plate, as expected, due to the higher tangential component of the gravitational force for higher angles. The obtained velocities are very similar for both measurement methods, which concludes that the MPT technique is a very good alternative for the measurement of rotational velocities for magnetic particles.

5. Conclusion

The novel method for the determination of the restitution coefficient by magnetic particle tracking technology was validated by the comparison of the obtained results with measurements performed by the already established particle image velocimetry method. This was proven for normal and oblique impacts, as the results for the CoR were very similar for the examined range of impact velocities and impact angles. For higher velocities than the examined velocities, the MPT technology should provide similar results in terms of quality of the data points. However, as the measurement frequency is fixed, the amount of data points for the same distance will decrease, when the velocity of the particles is higher. This would result in a more difficult detection of the impact point in the measurement data. If the approach of using the heights before and after the impact is used, the MPT technology could still provide good results for the coefficient of restitution, as the height can be analyzed by more data points than just one for the impact. Furthermore, the rotational behavior was also examined and it was shown that the results of both measurement techniques are similar, which allows to conclude that the MPT technology is suitable for the measurement of rotational velocities.
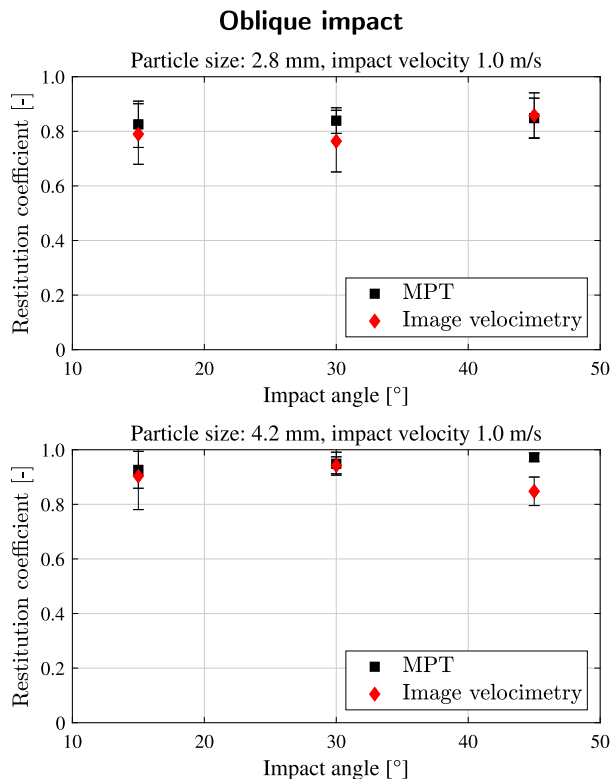
Even though MPT is only applicable for the tracking of magnetic particles, the method comes along with advantages in comparison to the classical methods. Contrary to high-speed imaging, where intense and homogeneous illumination of the particles must be ensured, for MPT no special requirements are needed, which makes the measurement and analysis faster and easier to handle. Another advantage is the 3D tracking of the tracer particle by MPT. For the conventional method at least two cameras would be necessary to enable the measurement of the 3D-movement of the particle. Furthermore, the high-speed cameras are usually able to measure the particle trajectory on a relatively short distance near contact point, whereas the MPT can record the whole drop experiment path of the particle.

In summary the MPT was proven to be a good alternative for the measurement of the restitution coefficient and the rotational velocity of magnetic particles. It was shown that the behavior of the tracer particle can be assumed to be equivalent to the bulk particles and that the analysis of the tracer represents the bulk behavior, which will be examined in detail in further experiments in the rotary granulator laboratory plant.

Declaration of Competing Interest

The authors declare that they have no known competing financial interests or personal relationships that could have appeared to influence the work reported in this paper.

Acknowledgment

References

[1] M.J. Adams, C.J. Lawrence, M. Urso, J. Rance, Modelling collisions of soft agglomerates at the continuum length scale, Powder Technol. 140 (2004) 268–279, https://doi.org/10.1016/j.powtec.2004.01.013.

[2] Andrä, W., Nowak, H. (Eds.), 2006. Magnetism in Medicine. Wiley-VCH Verlag GmbH & Co. KGaA, Weinheim, Germany. doi:10.1002/9783527610174.

[3] S. Antonyuk, S. Heinrich, N. Deen, H. Kuipers, Influence of liquid layers on energy absorption during particle impact, Particuology 7 (2009) 245–259, https://doi.org/10.1016/j.partic.2009.04.006.

[4] S. Antonyuk, S. Heinrich, P. Gurikov, S. Raman, I. Smirnova, Influence of coating and wetting on the mechanical behaviour of highly porous cylindrical aerogel particles, Powder Technol. 285 (2015) 34–43, https://doi.org/10.1016/j.powtec.2015.05.004.

[5] S. Antonyuk, S. Heinrich, J. Tomas, N.G. Deen, M.S. van Buijtenen, J.A.M. Kuipers, Energy absorption during compression and impact of dry elastic-plastic spherical granules, Granular Matter 12 (2010) 15–47, https://doi.org/10.1007/s10035-009-0161-3.

[6] F.G. Bridges, A. Hatzes, D.N.C. Lin, Structure, stability and evolution of saturn's rings, Nature 309 (1984) 333–335, https://doi.org/10.1038/309333a0.

[7] Buck, B., 2018. Influence of liquids on particle collision dynamics, Dissertation, TUHH. Cuvillier Verlag, Göttingen.

[8] B. Buck, S. Heinrich, Collision dynamics of wet particles: Comparison of literature models to new experiments, Adv. Powder Technol. 30 (2019) 3241–3252, https://doi.org/10.1016/j.apt.2019.09.033.

[9] B. Buck, J. Lunewski, Y. Tang, N.G. Deen, J. Kuipers, S. Heinrich, Numerical investigation of collision dynamics of wet particles via force balance, Chem. Eng. Res. Des. 132 (2018) 1143–1159, https://doi.org/10.1016/j.cherd.2018.02.026.

[10] B. Buck, Y. Tang, N.G. Deen, J. Kuipers, S. Heinrich, Dynamics of wet particle–wall collisions: Influence of wetting condition, Chem. Eng. Res. Des. 135 (2018) 21–29, https://doi.org/10.1016/j.cherd.2018.05.014.

[11] B. Buck, Y. Tang, S. Heinrich, N.G. Deen, J. Kuipers, Collision dynamics of wet solids: Rebound and rotation, Powder Technol. 316 (2017) 218–224, https://doi.org/10.1016/j.powtec.2016.12.088.

[12] K.A. Buist, A.C. van der Gaag, N.G. Deen, J.A.M. Kuipers, Improved magnetic particle tracking technique in dense gas fluidized beds, AIChE J. 60 (2014) 3133–3142, https://doi.org/10.1002/aic.14512.

[13] K.A. Buist, T.W. van Erdewijk, N.G. Deen, J.A.M. Kuipers, Determination and comparison of rotational velocity in a pseudo 2-d fluidized bed using magnetic particle tracking and discrete particle modeling, AIChE J. 61 (2015) 3198–3207, https://doi.org/10.1002/aic.14949.

[14] J. Coaplen, W.J. Stronge, B. Ravani, Work equivalent composite coefficient of restitution, Int. J. Impact Eng 30 (2004) 581–591, https://doi.org/10.1016/j.ijimpeng.2003.10.038.

[15] B. Crüger, S. Heinrich, S. Antonyuk, N.G. Deen, J. Kuipers, Experimental study of oblique impact of particles on wet surfaces, Chem. Eng. Res. Des. 110 (2016) 209–219, https://doi.org/10.1016/j.cherd.2016.01.024.

[16] S. Drücker, I. Krautstrunk, M. Paulick, K. Saleh, M. Morgeneyer, A. Kwade, Development of an experimental setup for the measurement of the coefficient of restitution under vacuum conditions, Journal of visualized experiments: JoVE (2016) e53299, https://doi.org/10.3791/53299.

[17] S. Golshan, R. Sotudeh-Gharebagh, R. Zarghami, N. Mostoufi, B. Blais, J. Kuipers, Review and implementation of cfd-dem applied to chemical process systems, Chem. Eng. Sci. 221 (2020) 115646, https://doi.org/10.1016/j.ces.2020.115646.

[18] P. Grohn, D. Weis, M. Thommes, S. Heinrich, S. Antonyuk, Contact behavior of microcrystalline cellulose pellets depending on their water content, Chemical Engineering & Technology 43 (2020) 887–895, https://doi.org/10.1002/ceat.201900517.

[19] A.P. Hatzes, F.G. Bridges, D.N.C. Lin, Collisional properties of ice spheres at low impact velocities, Mon. Not. R. Astron. Soc. 231 (1988) 1091–1115, https://doi.org/10.1093/mnras/231.4.1091.

[20] J. Hlosta, D. Žurovec, J. Rozbroj, Á. Ramírez-Gómez, J. Nečas, J. Zegzulka, Experimental determination of particle–particle restitution coefficient via double pendulum method, Chem. Eng. Res. Des. 135 (2018) 222–233, https://doi.org/10.1016/j.cherd.2018.05.016.

[21] S.M. Iveson, J.D. Litster, Liquid-bound granule impact deformation and coefficient of restitution, Powder Technol. 99 (1998) 234–242, https://doi.org/10.1016/S0032-5910(98)00115-6.

[22] A.A. Kantak, J.E. Galvin, D.J. Wildemuth, R.H. Davis, Low-velocity collisions of particles with a dry or wet wall, Microgravity - Science and Technology 17 (2005) 18–25, https://doi.org/10.1007/BF02870971.

[23] A.H. Kharaz, D.A. Gorham, A.D. Salman, An experimental study of the elastic rebound of spheres, Powder Technol. 120 (2001) 281–291, https://doi.org/10.1016/S0032-5910(01)00283-2.

[24] J. Kristensen, T. Schaefer, P. Kleinebudde, Direct pelletization in a rotary processor controlled by torque measurements. ii: effects of changes in the content of microcrystalline cellulose, AAPS pharmSci 2 (2000) E24, https://doi.org/10.1208/ps020324.

[25] H. Kruggel-Emden, E. Simsek, S. Rickelt, S. Wirtz, V. Scherer, Review and extension of normal force models for the discrete element method, Powder Technol. 171 (2007) 157–173, https://doi.org/10.1016/j.powtec.2006.10.004.

[26] F. Krull, J. Mathy, P. Breuninger, S. Antonyuk, Influence of the surface roughness on the collision behavior of fine particles in ambient fluids, Powder Technol. 392 (2021) 58–68, https://doi.org/10.1016/j.powtec.2021.06.051.

[27] J.C. Maxwell, A dynamical theory of the electromagnetic field, Philos. Trans. R. Soc. Lond. 155 (1865) 459–512, https://doi.org/10.1098/rstl.1865.0008.

[28] P. Müller, S. Antonyuk, M. Stasiak, J. Tomas, S. Heinrich, The normal and oblique impact of three types of wet granules, Granular Matter 13 (2011) 455–463, https://doi.org/10.1007/s10035-011-0256-5.

[29] P. Müller, R. Böttcher, A. Russell, M. Trüe, S. Aman, J. Tomas, Contact time at impact of spheres on large thin plates, Adv. Powder Technol. 27 (2016) 1233–1243, https://doi.org/10.1016/j.apt.2016.04.011.

[30] Neuwirth, J., 2016. Charakterisierung und Diskrete-Partikel-Modellierung des Strömungs- und Dispersionsverhaltens im Rotorgranulator. Dissertation. Technische Universität Hamburg-Harburg and Technische Universität Hamburg.

[31] J. Neuwirth, S. Antonyuk, S. Heinrich, M. Jacob, Cfd-dem study and direct measurement of the granular flow in a rotor granulator, Chem. Eng. Sci. 86 (2013) 151–163, https://doi.org/10.1016/j.ces.2012.07.005.

[32] Newton, I., 1687. Philosophiae naturalis principia mathematica. Jussu Societatis Regiae ac Typis Josephi Streater. Prostat apud plures bibliopolas. doi:10.5479/sil.52126.39088015628399.

[33] T. Pöschel, T. Schwager, Computational Granular Dynamics, Springer-Verlag, Berlin/Heidelberg, 2005, https://doi.org/10.1007/3-540-27720-X.

[34] W.H. Press, Numerical recipes: The art of scientific computing, 3. ed., Cambridge Univ. Press, Cambridge, 2007.

[35] H. Richert, O. Kosch, P. Görnert, Magnetic monitoring as a diagnostic method for investigating motility in the human digestive system, in: W. Andrä, H. Nowak (Eds.), Magnetism in Medicine, Wiley-VCH Verlag GmbH & Co. KGaA, Weinheim, Germany, 2006, pp. 481–498, https://doi.org/10.1002/9783527610174.ch4b.

[36] V. Salikov, S. Heinrich, S. Antonyuk, V.S. Sutkar, N.G. Deen, J. Kuipers, Investigations on the spouting stability in a prismatic spouted bed and apparatus optimization, Adv. Powder Technol. 26 (2015) 718–733, https://doi.org/10.1016/j.apt.2015.02.011.

[37] R. Seifried, W. Schiehlen, P. Eberhard, Numerical and experimental evaluation of the coefficient of restitution for repeated impacts, Int. J. Impact Eng 32 (2005) 508–524, https://doi.org/10.1016/j.ijimpeng.2005.01.001.

[38] R. Seifried, W. Schiehlen, P. Eberhard, The role of the coefficient of restitution on impact problems in multi-body dynamics, Proceedings of the Institution of Mechanical Engineers, Part K: Journal of Multi-body Dynamics 224 (2010) 279–306, https://doi.org/10.1243/14643191JMBD239.

[39] J. Seville, C.D. Willett, P.C. Knight, Interparticle forces in fluidisation: a review, Powder Technol. 113 (2000) 261–268, https://doi.org/10.1016/S0032-5910(00)00309-0.

[40] A.B. Stevens, C.M. Hrenya, Comparison of soft-sphere models to measurements of collision properties during normal impacts, Powder Technol. 154 (2005) 99–109, https://doi.org/10.1016/j.powtec.2005.04.033.

[41] V.S. Sutkar, N.G. Deen, J.T. Padding, J. Kuipers, V. Salikov, B. Crüger, S. Antonyuk, S. Heinrich, A novel approach to determine wet restitution coefficients through a unified correlation and energy analysis, AIChE J. 61 (2015) 769–779, https://doi.org/10.1002/aic.14693.

[42] V.S. Sutkar, N.G. Deen, A.V. Patil, V. Salikov, S. Antonyuk, S. Heinrich, J. Kuipers, Cfd–dem model for coupled heat and mass transfer in a spout fluidized bed with liquid injection, Chem. Eng. J. 288 (2016) 185–197, https://doi.org/10.1016/j.cej.2015.11.044.

[43] E. Teunou, D. Poncelet, Batch and continuous fluid bed coating – review and state of the art, J. Food Eng. 53 (2002) 325–340, https://doi.org/10.1016/S0260-8774(01)00173-X.

[44] M.S. van Buijtenen, N.G. Deen, S. Heinrich, S. Antonyuk, J.A.M. Kuipers, A discrete element study of wet particle-particle interaction during granulation in a spout fluidized bed, The Canadian Journal of Chemical Engineering 87 (2009) 308–317, https://doi.org/10.1002/cjce.20144.

[45] M.K. Vuppala, D.M. Parikh, H.R. Bhagat, Application of powder-layering technology and film coating for manufacture of sustained-release pellets using a rotary fluid bed processor, Drug Dev. Ind. Pharm. 23 (1997) 687–694, https://doi.org/10.3109/03639049709150770.

[46] E. Willert, S. Kusche, V.L. Popov, The influence of viscoelasticity on velocity-dependent restitutions in the oblique impact of spheres, Facta Universitatis, Series: Mechanical Engineering 15 (2017) 269, https://doi.org/10.22190/FUME170420006W.

[47] I. Yardeny, D. Portnikov, H. Kalman, Experimental investigation of the coefficient of restitution of particles colliding with surfaces in air and water, Adv. Powder Technol. 31 (2020) 3747–3759, https://doi.org/10.1016/j.apt.2020.07.018.